A Database for Simultaneous Observations of the Earth's Magnetosheath by Cluster and MMS Between 2017 and 2021

Costel Munteanu[1], Eliza Teodorescu[1], Marius Echim[1,2,3], Daniel Dumitru[1], Gabriel Voitcu[1], Maximilian Teodorescu[1]and Cătălin Negrea[1]

[1]Institute of Space Science - Subsidiary of INFLPR, Măgurele, Romania.
[2]The Royal Belgian Institute for Space Aeronomy, Brussels, Belgium.
[3]Belgian Solar Terrestrial Center of Excellence, Brussels, Belgium.

Key Points:

- We use in-situ measurements from Cluster 4 and MMS 4 to build a catalogue/database of simultaneous observations of the Earth's magnetosheath
- Empirical models and minimum variance analysis of the magnetic field allow for an estimation of the bow-shock orientation for each event
- We also provide details on the relative spacecraft position and an analysis of the bow-shock geometry

Corresponding author: Eliza Teodorescu, eliteo@spacescience.ro

Abstract

This paper describes a catalogue of simultaneous observations of the Earth's magnetosheath by ESA's Cluster and NASA's MMS missions. The catalogue is built from a visual inspection of summary plots provided by the two missions complemented by an analysis of high-resolution magnetic field data. The catalogue includes 117 events when Cluster 4 and MMS 4 crossed simultaneously the magnetosheath between January-April, 2017-2021. We also determine the bow shock geometry for each event based on two different approaches: a) a minimum variance analysis of in-situ magnetic field measurements, and b) a geometrical approach which considers a bow shock model parameterized by OMNI data. A description of spacecraft trajectory during each event is also provided. Additional data describe the relative distances between Cluster 4 and MMS 4, a classification of each event as either quasi-parallel or quasi-perpendicular, and the distribution of events per magnetospheric flank. The time intervals for the Cluster - MMS conjunctions included in the catalogue, as well as all associated figures and tables discussed in this paper are made available through an independent online data repository, and can be freely downloaded and used by any interested researcher.

1 Introduction

The Earth's magnetosphere acts as an obstacle to the supersonic solar wind flow, resulting in the formation of a bow shock which decelerates the solar wind to sub-magnetosonic speeds. The decelerated solar wind is then deflected around the magnetosphere, in the region between the bow shock and the magnetopause, called the magnetosheath (MSH) region. It is in this region where the actual interaction between the (shocked) solar wind and the Earth's magnetosphere takes place, thus, most processes related to the transfer of mass, momentum, and energy are strongly influenced by bow shock and magnetosheath properties. The magnetosheath also serves as a natural plasma laboratory, exhibiting various types of wave activity, turbulent fluctuations, small-scale structures and transient phenomena in response to changes in the solar wind and interplanetary magnetic field (e.g., Narita et al., 2021; Echim et al., 2021, 2023).

The Earth's MSH region and its boundaries were extensively studied using single-spacecraft observations (e.g., Song & Russell, 1997). In the past two decades, an increasingly large number of publications use data from multi-spacecraft missions like Cluster (Haaland et al., 2014; Kruparova et al., 2019; Haaland et al., 2021), THEMIS (Dimmock & Nykyri, 2013; Haaland et al., 2019) or MMS (Paschmann et al., 2018; Haaland et al., 2020). Kruparova et al. (2019), for example, compiled a list of more than 500 bow shock crossings observed by Cluster in 2001-2013; they used timing methods applied to multi-point measurements, and studied spatio-temporal features of the bow shock. Such multi-spacecraft missions are an invaluable resource, but the relatively small inter-spacecraft separations limits investigations to only local processes or events. Simultaneous observations of MSH allowing investigation of dawn-dusk asymmetries, for example, are not possible using observations from only one spacecraft constellation. To our knowledge, there are very few studies reporting simultaneous MSH observations from multiple spacecraft constellations. Nevertheless, Escoubet et al. (2020), use a simultaneous Cluster-MMS crossing of the magnetopause to investigate the magnetospheric impact of high-speed MSH jets.

The dynamical and turbulent features of the magnetosheath are strongly influenced by θ_{Bn}, the angle between the interplanetary magnetic field (IMF) and the shock normal direction. When θ_{Bn} takes values close to zero the shock is called quasi-parallel ($Q_{\parallel}$, see, e.g., Schwartz & Burgess, 1991); when θ_{Bn} takes values close to 90 degrees the shock is called quasi-perpendicular ($Q_{\perp}$, e.g., Karlsson et al., 2021). Generally, a $Q_{\parallel}$ shock is associated with the dawn flank of the MSH while a $Q_{\perp}$ shock is more often found in the dusk flank. A $Q_{\parallel}$ shock is characterized by a wide transition region between supersonic

and subsonic flow and is often perturbed by upstream waves and instabilities (see, e.g., Leroy et al., 1982; Krasnoselskikh et al., 2013). In contrast, $Q_\perp$ shocks are characterized by sharp transitions from the solar wind to the MSH (e.g., Plank & Gingell, 2023). The MSH behind a $Q_\parallel$ shock exhibits strong turbulence, with magnetic fluctuation levels $\delta B/B$ close to unity, while the magnetic field fluctuations behind a $Q_\perp$ bow shock are about one order of magnitude weaker (e.g., Schwartz & Burgess, 1991). A recent review of turbulence and complexity in key magnetospheric regions, including the MSH, can be found in Echim et al. (2021).

Asymmetries between the two flanks of the MSH, concerning the density or the velocity, have been reported decades ago (Walters, 1964) and confirmed by several more recent studies (Walsh et al., 2012; Dimmock et al., 2016). Further, similarities but also differences between the properties of turbulence have also been demonstrated both in the two flanks and with respect to the bow shock geometry. (Shevyrev et al., 2006) or (Breuillard et al., 2018) show that Kolmogorov-like spectral properties (Kolmogorov, 1941), characteristic to developed turbulence, are present downstream $Q_\parallel$ MSH at scales similar to an inertial range. The inertial regime is also found in the flanks of the MSH and closer to the magnetopause (Alexandrova et al., 2008; Huang et al., 2017; Teodorescu & Echim, 2020) while a steepening of the spectral scaling can be evidenced from behind the bow shock (Czaykowska et al., 2001; Dwivedi et al., 2019) towards the magnetopause (Sahraoui et al., 2006). In a recent study, Teodorescu et al. (2021) show that an inertial regime of scales is present in the MSH even behind $Q_\perp$ shocks, suggesting that the solar wind turbulence might cross the $Q_\perp$ shock. At ion scales, turbulence properties seem not to depend on the bow shock orientation (Li et al., 2020; Rakhmanova et al., 2021), although various spectral indices have been reported (Smith et al., 2006).

Several approaches allow to estimate the geometry of the shock. Among the most commonly used is the minimum variance analysis applied on magnetic field data (MVAB; Sonnerup & Scheible, 1998); it estimates the orientation of a shock or discontinuity from in-situ observations. Mailyan et al. (2008) (see also Munteanu et al., 2013) used MVAB to estimate normal direction of a large set of solar wind discontinuities, and then used the results to calculate the solar wind propagation delay between ACE, the solar wind monitor at L1, and Cluster, the magnetospheric mission orbiting Earth. MVAB is also widely applied to find the orientation of the Earth's magnetopause and bow shock. Echim et al. (2024), for example, rotated multiple data sets (from global MHD, local-kinetic Vlasov and in-situ MMS2 observations associated with the same magnetopause crossing) into the same (MVAB-based) local coordinate system, allowing for a direct comparison between model results and in-situ observations.

Another common approach to estimate the geometry of the Earth's bow shock is from geometrical considerations. The global three-dimensional shape and position of the bow shock are estimated from a model parameterized by upstream solar wind conditions. Tátrallyay et al. (2012), determined that the bow shock position and shape are best predicted by the model of Farris et al. (1991) combined with Farris and Russell (1994). The latter is used in this study to determine the bow shock orientation and then compute the angle, θ_{Bn}, between the normal to the model shock surface and the direction of the IMF. Other methods to determine bow shock orientation involve multi-spacecraft recordings. Four-point magnetic field measurements from Cluster were used by Shen et al. (2007) to develop a new approach to determine the normal direction to the Earth's bow shock. Recently, Karlsson et al. (2021) introduced yet another approach based on pairs of Cluster spacecraft during intervals when one spacecraft is located in the solar wind, and the other in the MSH, eliminating thus the uncertainties associated with propagating upstream measurements.

The MSH region is highly variable, thus, a large number of observations is needed to obtain a statistically significant result. Due to their longevity and orbital characteristics (e.g., the apogees of both constellations are in the same region), Cluster and MMS

are good candidates to provide such joint observations. We are aware of only one attempt to compile a database of simultaneous Cluster-MMS magnetosheath observations, which is briefly discussed by Escoubet et al. (2020). Figure 13b in their paper illustrates a set of predicted Cluster-MMS (and THEMIS) magnetosheath conjunctions for a time interval between 2020 and 2022. The global shape and position of their bow shock and magnetopause are estimated from models (...); the authors report a list of common MMS and Cluster observations of the MSH resulting from computing the intersection of the model boundaries with predicted spacecraft orbits. An updated and extended version of this catalogue is available at https://www.cosmos.esa.int/web/csa/mms-themis-conjunctions. Compared to this model-based catalogue, our database is fully data-driven, consequently, possible errors due to inaccurate estimates of model bow shock or magnetopause are reduced.

In this paper we describe the main elements included in a catalogue of simultaneous Cluster-MMS observations of the Earth's MSH region. The catalogue consists of 117 MSH crossing events between January-April, 2017-2021. The entire time span covers more than 5 years and is centered on the solar cycle minimum in 2019 which ensures that solar cycle effects due to, e.g., solar cycle variation of solar wind (and implicitly magnetosheath) properties, are reduced. We use two independent, but often complementary methods to estimate bow shock orientation: a) a minimum variance analysis of the magnetic field and b) a geometrical approach considering a bow shock model parameterized using OMNI solar wind data.

The paper is organized as follows. In Section 2 we provide a brief description of the data sets used in this study and the methodology used to identify Cluster and MMS magnetosheath crossings. In Section 3 we illustrate the two approaches adopted to estimate the bow shock orientation: (a) the minimum variance analysis of the magnetic field data and (b) a geometrical approach based on a bow shock empirical model parameterized with OMNI data. Section 4 presents the main characteristics of the catalogue built to present the results of simultaneous Cluster and MMS magnetosheath crossings in 2017-2021; we discuss here the bow shock type associated with each event. This section also includes a detailed account of spacecraft trajectories, which greatly expands the utility of our catalogue. Section 5 summarizes the results.

2 Identification of Magnetosheath Crossings from Cluster and MMS Data

Cluster is a four-spacecraft mission launched by ESA in 2000 (Escoubet et al., 2001). It has an elliptical polar orbit ($\sim 90°$ inclination), with perigee at 4 Re geocentric distance (1 Re = 6,371 km), apogee at 20 Re, and an orbital period of ~ 57 hr. The MSH crossings of Cluster4 (C4) spacecraft are determined by visual inspection of official summary data plots from Cluster (http://www.cluster.rl.ac.uk/csdsweb-cgi/csdsweb_pick). For MVAB, we use spin resolution (4 s) data from the fluxgate magnetometer onboard C4 (Balogh et al., 2001; Balogh & Lucek, 2021).

The Magnetospheric Multiscale (MMS) is a four-spacecraft mission launched by NASA in 2015 (Burch et al., 2016). It has a highly elliptical equatorial orbit ($\sim 28°$ inclination), with perigee at 1.2 Re, apogee at 25 Re, and an orbital period of about 66 hr (Fuselier et al., 2016). Magnetosheath crossings of MMS4 (M4) spacecraft are determined by visual inspection of official summary data plots from MMS (https://lasp.colorado.edu/mms/sdc/public/plots/#/quicklook). In addition, we also inspect the MMS "Historical Orbit Plots" (https://lasp.colorado.edu/mms/sdc/public/plots/#/historical-orbit). For MVAB, we use survey (8 or 16 Samples/s) data from the fluxgate magnetometer onboard M4 (Russell et al., 2016, 2022).

The bow shock empirical model (Farris et al., 1991; Farris & Russell, 1994) uses OMNI data as input. The OMNI dataset consists of solar wind magnetic field and plasma observations time-shifted to the location of the Earth's bow shock nose (King & Papitashvili, 2005); see also: https://omniweb.gsfc.nasa.gov/html/HROdocum.html. We use the high-resolution (1 m) OMNI data from Papitashvili and King (2020).

We identify the time intervals when the spacecraft crosses the magnetosheath by visual inspection of summary plots. Ion energy spectra help identify the solar wind (ion energy is usually concentrated in a very narrow band around 1 keV) and the magnetosheath (a large spread in ion energy values is observed). Other typical signatures of the magnetosheath crossings are found in magnetic field observations. Indeed, typical interplanetary magnetic field at 1 AU is characterized by relatively small-amplitude fluctuations around an average magnitude usually less than $\sim$ 10 nT. As a spacecraft approaches Earth, it will cross the bow shock and enter the magnetosheath, where the magnetic field variability is much larger. As the spacecraft further advances towards the Earth, it will cross the magnetopause and enter the magnetosphere, where the level of magnetic fluctuations decreases and the average field magnitude increases significantly. A more detailed account of magnetic field changes as Cluster crosses through various plasma regions around Earth can be found in Dumitru and Munteanu (2023).

2.1 Magnetosheath Crossings From Cluster

Figure 1 shows a summary data plot from Cluster. The figure depicts the 6 hr interval 06:00-12:00 UTC, on 2017-04-20. The magnetosheath interval is clearly identifiable in the ion energy spectrum during $\sim$ 07:00-11:50 UTC. Before 07:00, the ion energies are concentrated within a narrow band around 1 keV, signifying that the spacecraft is in the solar wind. At 07:00, a rapid spread in ion energies is observed, signifying the bow shock crossing. At 11:50 the ion energy flux decreases, signifying the crossing of the magnetopause. Two sharp changes in ion energy flux are observed at 07:10 and 07:45 UTC; these are artifacts created by changes in instrument operation mode. At 07:10 the measurement mode changed from "14" (Compression MAG-4 + 3Ds sheath/tail) to "8" (Magnetosphere 1). This resulted in an artificial increase in energy flux. At 07:45 the instrument sensitivity changed from low- to high-sensitivity. This resulted in a strong decrease (2 orders of magnitude) in ion E-flux. Details about Cluster-CIS operation modes and measurement sensitivities can be found in Rème et al. (2001).

Magnetic field signatures typical for MSH are not obvious in Fig. 1 top panel. The bow shock crossing, identified by the sharp increase in magnetic field strength at 07:00 UTC is clear, but the magnetopause crossing is not evident in this example. The orbit plots (Fig. 1 top-right) confirm that the spacecraft is on the dayside, mostly within the magnetosheath model boundaries. A more detailed account on magnetic field observations and spacecraft trajectory for this event are given in Sections 3 and 4.

All Cluster summary data plots available from January to April for each year, starting from 2017 to 2021, were inspected, and all orbits revealing clear MSH intervals were selected for further analysis. We also performed a data inspection for MMS data summary plots in a similar fashion as that described for Cluster and further detailed in the next section.

2.2 Magnetosheath Crossings From MMS

Figure 2 shows an MMS data summary plot for 2017-04-20. The magnetosheath crossing is clearly identified by the interval of increased H+ energy counts in the range 100-10000 eV, during $\sim$ 07:00-14:00 UTC. Before 07:00, the H+ energies are concentrated in a narrow band centered on 1000 eV, signifying that the spacecraft is in the solar wind. At 07:00, the H+ energy depicts a rapid spread in values, signifying the bow shock cross-

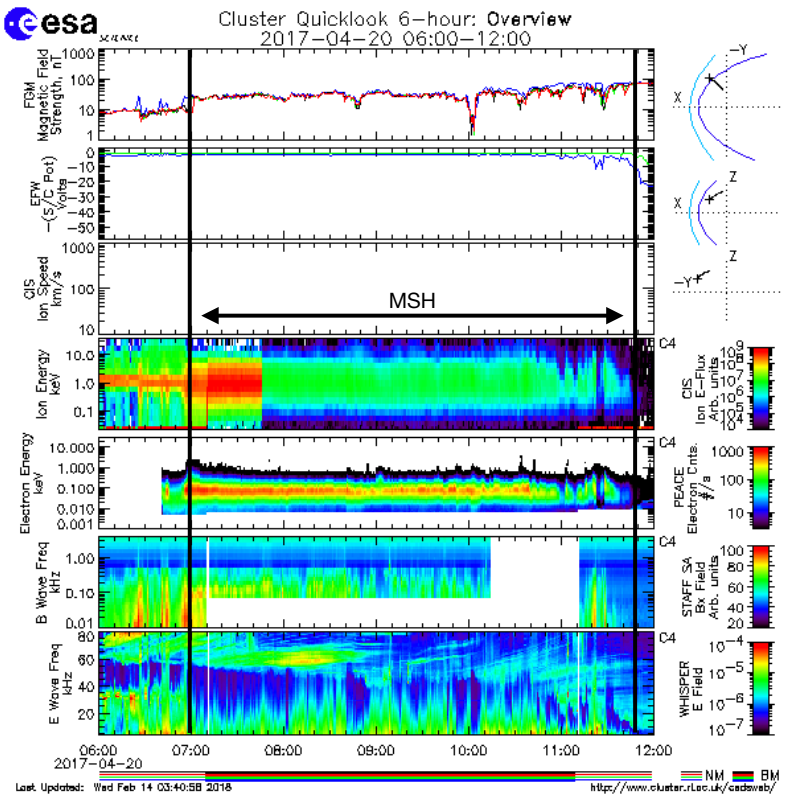

Figure 1. Cluster data summary plot: 6-hour data overview, between 06:00-12:00 UTC on 2017-04-20. From top to bottom: magnetic field strength (nT), EFW (Volts), CIS ion speed (km/s), ion energy (keV), electron energy (keV), B wave frequency (kHz) and E wave frequency (kHz). The magnetosheath interval (from ∼07:00 to 11:50) is marked across all panels. Top-right: GSE spacecraft trajectory; light blue depicts model bow shock and model magnetopause is in dark blue. Image downloaded from http://www.cluster.rl.ac.uk/csdsweb-cgi/csdsweb_pick.

ing. At 14:00, the ion H+ count in the range 100-10000 eV decreases, signifying the crossing of the magnetopause. Figure 2 also depicts the O+ energy spectrum; the crossing of the magnetopause is easily identifiable by the sharp decrease in O+ flux in the range 100-10000 eV at 14:00, followed by a significant increase of this flux at energies above 10000 eV.

In this example, the magnetosheath crossing is clearly identifiable also from magnetic field observations (Fig. 2, top panel). Relatively low-amplitude magnetic fluctuations and an average magnetic field magnitude around 10 nT are observed before 07:00 UTC. The sharp increase of magnetic field magnitude at this point marks the crossing through the bow shock, and the comparatively much larger field fluctuations between 07:00-14:00 correspond to typical magnetosheath observations. The rapid decrease of field fluctuations, followed by a systematic increase of field magnitude as the spacecraft moves closer to Earth, indicate the transition through the magnetopause. The GSE trajectory of the spacecraft is also included in Fig. 2: at 04:00 UTC the spacecraft is located at R=21.4 Re, and reaches a 5.3 Re geocentric distance at 00:00 on 2007-04-21.

In addition to data summary plots, we also inspect MMS historical orbit plots (not shown here). These plots include an illustration of the spacecraft trajectory relative to a model magnetopause. We searched for time intervals which include MMS measurements

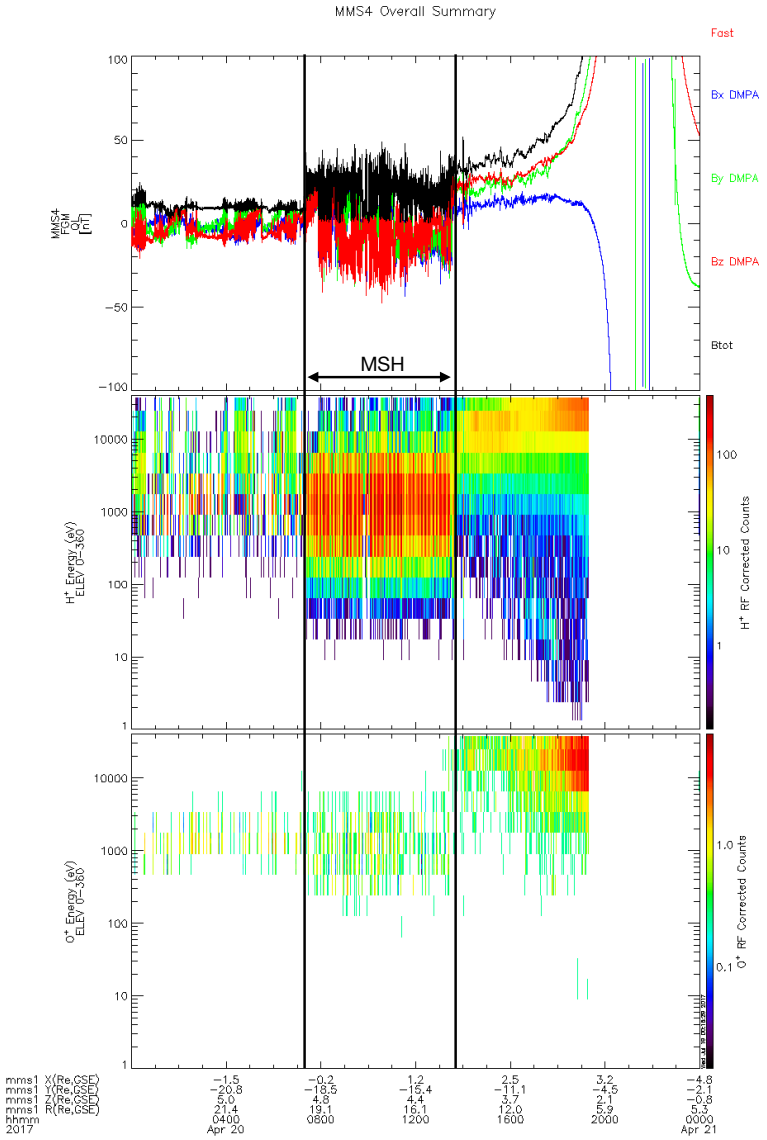

Figure 2. MMS4 data summary plot for April 20, 2017. From top to bottom: magnetic field (nT); H+ energy (eV), and O+ energy (eV). The magnetosheath interval (from ∼ 07:00 to 14:00 UTC) is marked across all panels. In addition to UTC time, the x-axis also shows the GSE trajectory of the spacecraft. Image downloaded from https://lasp.colorado.edu/mms/sdc/public/plots/#/quicklook.

that show some overlap with the Cluster MSH traversals determined in the previous step. A minimum common MSH observation time of one hour between the two spacecraft is required for the time interval to be included in our database. This selection criterion results in the determination of 117 events of simultaneous MSH crossings by C4 and M4 spacecraft during 2017-2021.

3 Estimation of Bow Shock Orientation

Earth's bow shock geometry is defined to be quasi-parallel or quasi-perpendicular, depending on the angle θ_{Bn}, between the IMF and the bow shock normal direction. The IMF is determined from OMNI data and the direction of the normal to the bow shock is estimated through two independent approaches: a) a minimum variance analysis applied on magnetic field in-situ measurements at the time of the bow shock crossing and b) an empirical model of the bow shock shape and position which allows for an estimation of the bow-shock geometry for each time stamp of the entire MSH crossing.

Minimum variance analysis of the magnetic field is the most frequently used method to obtain the orientation of a discontinuity based on a one-dimensional model of a current sheet. From in-situ magnetic field measurements during the transversal of the discontinuity, one finds the normal direction to the discontinuity as the direction defined by the minimum variance of the magnetic field. Mathematically, this is achieved by constructing a magnetic covariance matrix and thereafter finding the eigenvectors and eigenvalues of this matrix (Sonnerup & Scheible, 1998). In this work we use a covariance matrix of the form discussed by Mailyan et al. (2008) and Munteanu et al. (2013).

A well known alternative method to estimate bow shock orientation is based on empirical models (Tátrallyay et al., 2012). We follow these lines and estimate the bow shock global 3D shape and position based on the model proposed by Farris et al. (1991) parameterized with in-situ OMNI solar wind data. Thus, θ_{Bn} is estimated as the angle between the normal to the model bow shock, computed for a position chosen as the median of Cluster's or MMS' coordinates during the entire MSH crossing, and each IMF measurement recorded in the time-intervals during which Cluster and MMS cross the MSH, respectively. This procedure results in a time-series of θ_{Bn} that evidences how the MSH geometry configuration changes with the IMF orientation, considering a fixed normal and bow shock during the entire crossing (Teodorescu et al., 2021).

We decided to apply both approaches since each method proves to be relevant depending on the type of analysis that is envisaged. For example, MVAB could be more accurate for analyses that concentrate on phenomena at/or near the bow shock while the estimation of θ_{Bn} fluctuations during longer periods of time might prove more useful when trying to characterize an entire sector of the MSH.

3.1 Bow Shock Orientation Using MVAB

Figure 3 illustrates an example of how one estimates bow shock orientation using the minimum variance analysis of the magnetic field (MVAB). Figure 3a depicts an interval of two days of total magnetic field measurements from C4 and M4, starting on 20-04-2017. Magnetosheath intervals are identified by large-amplitude magnetic field fluctuations with sharp boundaries on each side, separating them from the comparatively low-amplitude fluctuations in the solar wind and magnetosphere. The first half of the interval depicted in Fig 3a corresponds to inbound crossings for both spacecraft. Note that there is another set of magnetosheath crossings during the second half of the interval depicted in Fig 3a. During this second set of (outbound) crossings, C4 is seen exiting the magnetosheath, through a very well defined bow shock at about 14:00 UTC on 21-04-2017, while around the same time, M4 crosses the magnetopause entering the magnetosheath. Consequently, the magnetosheath observations by MMS and Cluster do not overlap, and this second set of crossings is not included in our catalogue. The simultaneous crossing event on 20-04-2017 is denoted as 201704ev09 in our catalogue. A figure similar to Fig. 3 is created for each of the 117 events included in our catalogue, available from the public repository acknowledged at the end of the paper.

C4 crossed the MSH on April 20 between 07:00-11:50 UTC. Figure 3b depicts C4 magnetic field observations during a 10 min window centered on the bow shock cross-

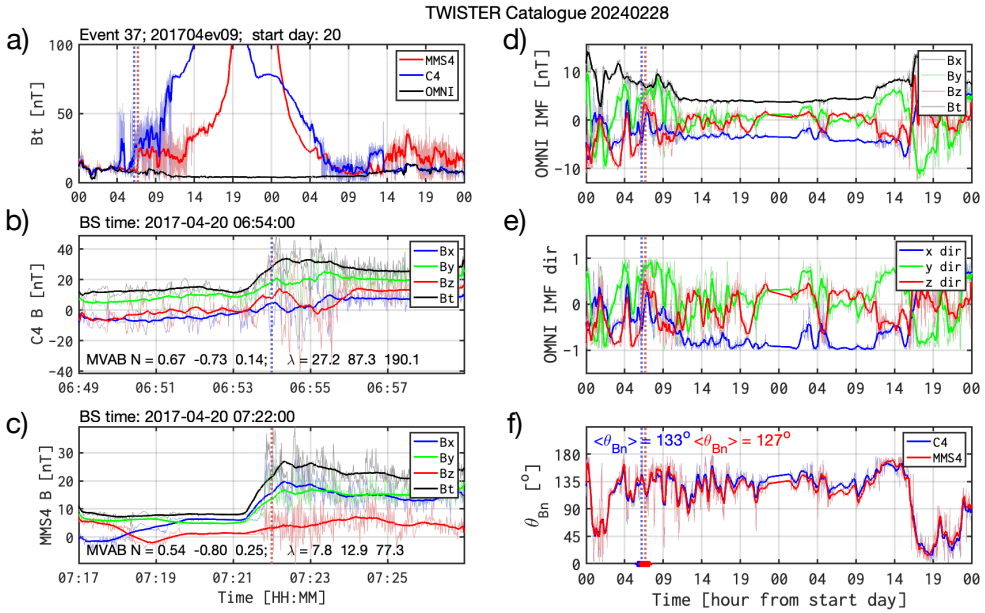

Figure 3. Estimating the bow shock orientation with a minimum variance analysis. (a) Magnetic field intensity from C4 (in blue) and M4 (in red) for a two-day interval starting on April 20, 2017; the vertical dotted lines mark the bow shock crossings. (b) and (c) Magnetic field data windows centered on the bow shock crossing for C4 and M4, respectively. (d) and (e) OMNI IMF data and IMF direction, respectively, for the same interval as in (a). (f) Time series of instantaneous θBn; thick lines at the bottom mark averaging intervals. This event is listed "201704ev09" in our catalogue, which includes similar figures for each of the 117 events.

ing at 06:54. MVAB applied on this data window results in a normal direction characterized by the following cosine angles (in GSE): $N_{C4} = [0.67, -0.73, 0.14]$. As a quality check for MVAB results, we compute the ratio between the intermediate and the smallest eigenvalues of the covariance matrix. In this example, this ratio is equal to $EvR \approx 87/27 = 3.22$, thus the normal estimation is quite accurate (Mailyan et al., 2008).

During the same day, M4 crosses the MSH for a slightly longer time interval, between 07:00-14:00 UTC. Nevertheless, the bow shock crossings of M4 and C4 are very close to each other (Fig. 3a). Figure 3c depicts M4 magnetic field observations during a 10 min window centered on the bow shock crossing at 07:22. MVAB gives a normal direction characterized by the cosine angles (in GSE) $N_{M4} = [0.54, -0.80, 0.25]$, and a corresponding eigenvalue ratio equal to $EvR \approx 12/7 = 1.7$. This value of EvR is less than 3, meaning that the normal is affected by errors. The angle between the MVAB normals computed for M4 and C4 is rather small ($\sim 10°$); this is consistent with the fact that the two spacecraft are in the same magnetospheric flank.

Figures 3d and 3e show the IMF OMNI data for the same 2-day interval as in Fig. 3a. The IMF shows large fluctuations of the magnetic intensity around 10 nT which cease around 12:00 UT on 20-04-2017 (Fig. 3d); then the IMF is stable with very low-amplitude fluctuations around an average intensity of 5 nT. This pattern is retrieved for the components indicating the IMF direction (Fig. 3e), which shows large fluctuations until 12:00 UT, then the fluctuations disappear almost completely, until 12:00 UT the next day (April 21). Between 04:00 UT and 12:00 UT on April 20, the IMF is strongly non-radial, with By-GSE being the main component (see Fig. 3e). However, at 12:00 UT on April 20 the

IMF direction changes to radial with Bx-GSE being the main component. Around 04:00 UT, we observe two strong southward excursions of the IMF direction.

Figure 3f shows the time series of θ_{Bn}, i.e. the angle between the normal to the bow shock computed with MVAB and the instantaneous IMF direction from OMNI data; θ_{Bn} takes values between 0° and 180°. We also compute an average θ_{Bn} estimated over one hour time intervals centered on each bow shock crossing (Fig. 3f). A MSH crossing event is considered quasi-perpendicular ($Q_\perp$) if the average θ_{Bn} takes values between 45° and 135°; the crossing is considered quasi-parallel ($Q_\parallel$) if θ_{Bn} is smaller than 45° or larger than 135°. As expected, θ_{Bn} follows very closely the variations in IMF direction.

Between 02:00 UT and 12:00 UT the instantaneous θ_{Bn} fluctuates strongly around 135°. The one-hour average computed for the time interval when the spacecraft cross the bow shock is equal to 133° for C4 and 127° for M4. On a closer inspection, the two southward excursions of IMF direction (when Bz is the main component of the IMF) around 04:00 are seen to correspond to θ_{Bn} larger than 135°, i.e., the bow shock is $Q_\parallel$. At 04:00 UT, the geometry is $Q_\perp$ (θ_{Bn} is around 90°), and we have pure non-radial IMF. At 07:00 UT, the IMF direction changes from southward (Bz dominated) to non-radial (By dominated), and this corresponds to a change from $Q_\parallel$ ($\theta_{Bn} > 135°$) to $Q_\perp$ ($\theta_{Bn} < 135°$) geometry. Although the main focus of our paper is to describe the database we created for simultaneous Cluster-MMS magnetosheath crossings, the instantaneous changes of bow shock geometry are relevant, and can be investigated from the information we provide in the catalogue figures, like in the example shown in Figure 3.

3.2 Determining the Bow Shock Orientation from Geometrical Considerations and Global Models of the Shock

In addition to the MVAB method, we also apply a geometrical approach to estimate θ_{Bn}. The results are included in the database and an example is illustrated in Figure 4 which shows the time-series of IMF, solar wind speed, v_{SW}, bow shock nose (BSN), solar wind pressure (P) and the plasma β.

An empirical two-dimensional model (Farris et al., 1991) estimates the bow shock radial distance, R_{BS} as:

$$R_{BS} = R_{BS_0} \frac{(1+\epsilon)}{1+\epsilon\cos\theta}, \tag{1}$$

where ϵ and θ are the solar zenith angle and the eccentricity, respectively, and R_{BS_0} is the radial distance at the bow shock nose provided by the OMNI data. The bow shock curves given in the X-R representation, where $R = \sqrt{(Y^2 + Z^2)}$, are shown in Fig. 4c.

To estimate the normal to the bow shock we need to estimate a position on the bow shock curve that is best correlated to the measurements recorded inside the MSH by the two probes, C4 and M4. An examination of the orbits of the two satellites lead us to conclude that: the starting point of the MSH crossing coordinates for Cluster and the median of the MSH crossing coordinates for MMS, are the best choices. The blue and red straight lines perpendicular to the bow shock curves illustrate the chosen positions in Fig. 4c. The blue and red curves in Fig. 4c show the simultaneous Cluster and MMS MSH crossings for event 201704ev09. For a clearer view of the MSH crossings, spacecraft trajectories in X-Y, X-Z and Y-Z coordinates are also provided (Figs. 4d, 4e and 4f, respectively).

In order to capture the variation of θ_{Bn} with the changes of the IMF direction, we compute the angle between the normal to the bow shock that is assigned to the entire MSH crossing of either Cluster or MMS and each measurement of the IMF recorded during the considered MSH crossing. The time variation of θ_{Bn}, due to changes of the IMF

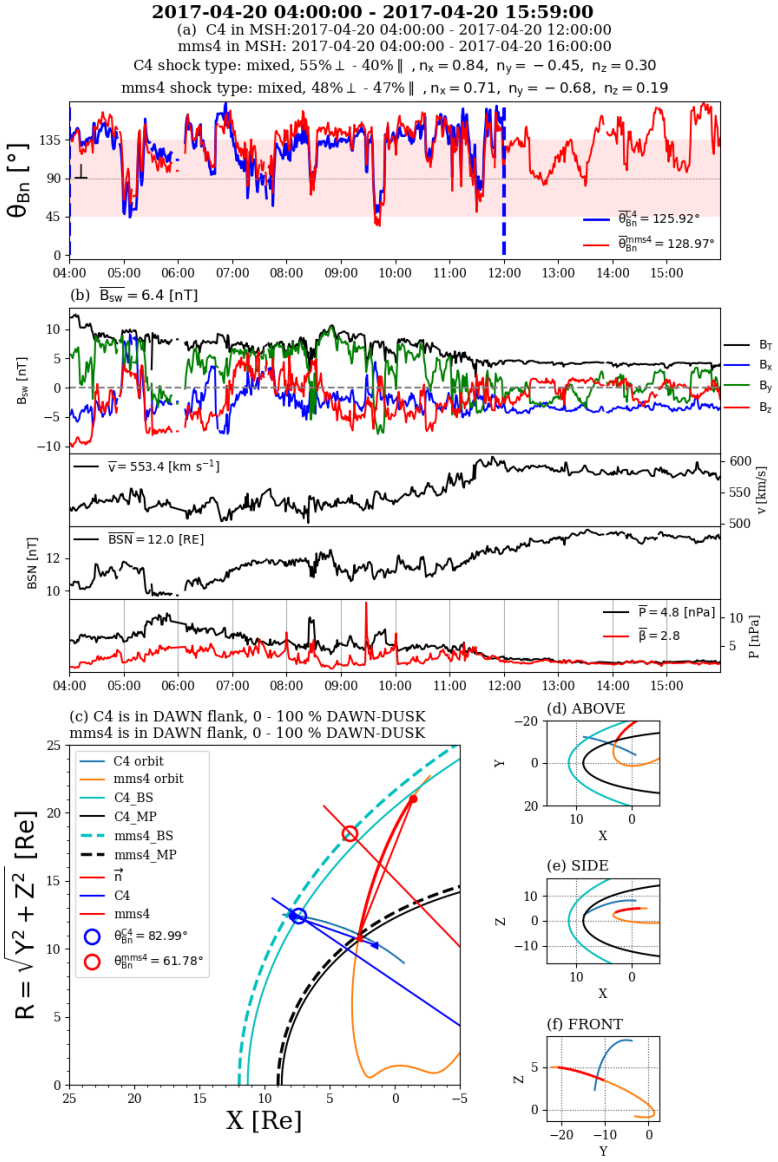

Figure 4. Estimating bow shock orientation using geometrical considerations and empirical models of the bow shock. a) θ_{Bn} time-series for event 201704ev09; C4 is in blue and M4 is in red. b) From top to bottom: IMF (nT), flow speed (km/s), bow shock nose location (Re) and flow pressure (nPa) from OMNI. c) Model bow shock and magnetopause (cyan and black curves, respectively) and C4/M4 MSH crossings (blue/red curves) projected onto R-X GSE plane; straight lines depict normal directions to the bow shock model at start/median positions of C4/M4 during the entire MSH crossing.

direction, is provided in Fig. 4a. Values that are inside/outside of the red-shaded area are $Q_\perp/Q_\parallel$. If more than 85% of the θ_{Bn} time-series points are inside/outside of the shaded area, the event is labeled as being $Q_\perp/Q_\parallel$. If less than 85% of the data satisfy this criterion, the event is labeled as "mixed" geometry; the percentages of $Q_\parallel$ and $Q_\perp$ are also indicated on the figure. For event 201704ev09, the MSH is in a mixed geometry for both satellites. Although, By is the dominant component during most of the MSH crossings, suggestive of a $Q_\parallel$ geometry, there are several reversals of its orientation, e.g. the inter-

val around 08:30 UT, that result in a change of geometry from $Q_{\parallel}$ to $Q_{\perp}$. The average values of θ_{Bn} are computed for both spacecraft, and are equal $\sim 125°$ for Cluster and $\sim 128°$ for MMS, in good agreement with the MVAB results for this particular event.

4 A Catalogue of Cluster-MMS Common Observations of the Magnetosheath Between 2017 and 2021

Due to the orbital characteristics, the Cluster quartet enters the upstream solar wind during January-April each year. The MMS quartet has an equatorial orbit allowing sweeping of the magnetosheath. Our study covers the period between January-April, from 2017 to 2021. The methodology described in Section 3 provides a number of 117 common MSH traversals during the targeted time interval. Table 1 shows the distribution of common MMS-Cluster crossings for each year and month. The full list of time intervals is available from our catalogue (Munteanu & Teodorescu, 2024), see also: http://www.spacescience.ro/projects/twister.

We included in the database the Cluster and MMS magnetosheath crossings that show at least 1 hour of common observations by the two spacecraft. There are well known difficulties in determining the exact bow shock and magnetopause locations, due to rapid back-and-forth movements of these boundary layers generated by solar wind variability. To avoid these difficulties, each interval in our catalogue is extended by about 1 hour before and after each boundary crossing time.

We report here only the simultaneous MSH crossings by the C4 and M4 spacecraft, but, due to the small inter-spacecraft separation within each quartet, the catalogue can be easily extended to all other pairs of Cluster-MMS spacecraft. The model-based catalogue available from https://www.cosmos.esa.int/web/csa/mms-themis-conjunctions, mentioned in the Introduction, for example, reports conjunctions between C4 and MMS1.

4.1 An Overview of MMS and Cluster Trajectories for the Events Included in the Database

Figure 5 shows the spacecraft trajectories in the GSE reference frame for all events identified in April 2017. Thirteen simultaneous MSH crossings are identified for C4 and M4 spacecraft during this period. Figure 5 illustrates the position of the spacecraft when it enters and when it exits the magnetosheath. For event no. 9, discussed in the previous sections, Fig. 5 shows that both spacecraft are located on the dayside, in the dawn flank, and above the ecliptic plane (X $>$ 0 RE, Y $<$ 0 and Z $>$ 0; Fig. 5a, 5b and 5c, respectively). Also, for the same event, the C4 radial distance from Earth decreases from 15 to about 10 RE, while for M4, R decreases from 20 to 10 RE (Fig. 5d).

Table 1. Number of events distributed per year/month.

Year	Jan	Feb	Mar	Apr	Total
2017	15	4	9	13	41
2018	4	6	6	8	24
2019	2	4	5	7	18
2020	6	3	1	5	15
2021	7	5	2	5	19
Total	34	22	23	38	117

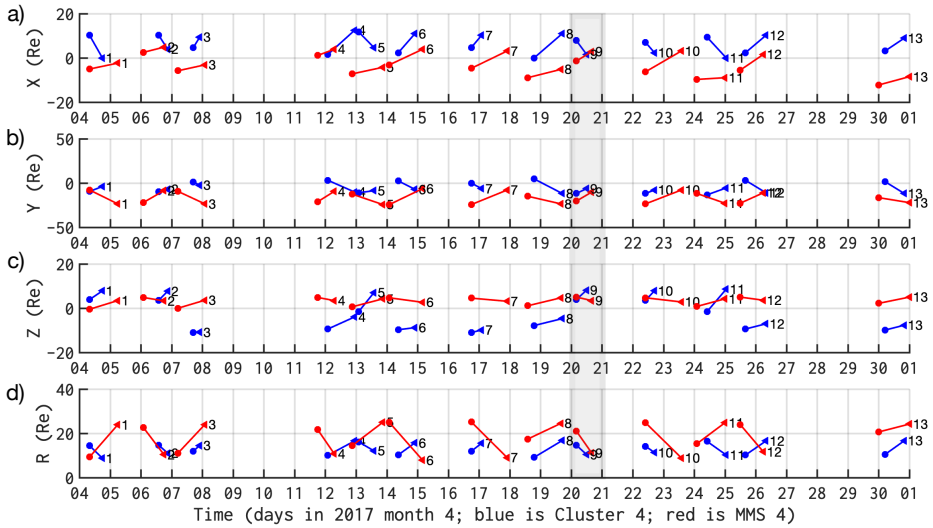

Figure 5. The simultaneous C4-M4 magnetosheath crossings identified in April 2017. From the top: X, Y, Z GSE spacecraft coordinates, and the total geocentric distance R, in RE. Time is depicted as day-of-month; C4 is in blue and M4 is depicted in red; circles depict entry in the magnetosheath and triangles indicate the exits from the magnetosheath. The crossings are indexed; event no. 9, which is the event illustrated in all previous figures, is highlighted. The catalogue includes similar figures for each month in our database.

Figure 5a reveals that all Cluster magnetosheath crossings in April 2017 took place at the dayside; also, almost all events from MMS have either one or both entry/exit points at negative X GSE, signifying that M4 spacecraft crosses the MSH deep in the flanks. Fig. 5b reveals that C4 often crosses from one flank to the other, while M4 is mostly located in the dawn flank.

Figure 5d shows the time variation of the total geocentric distance R, and these results can be used to identify the type of MSH crossing; three events are associated with simultaneous inward crossings of both spacecraft, and an equal number of events are simultaneous outward crossings. The rest of seven events correspond to different crossing directions for C4 and M4, with one being inward while the other one is outward, and vice-versa. These mixed crossing events signify that while one spacecraft is at the magnetopause, the other one is close to the bow shock (entering the MSH from the solar wind side).

Event no. 9, discussed in previous sections, is an example where both spacecraft cross the magnetosheath inward, meaning that C4 and M4 observe simultaneously the magnetopause and the bow shock.

A description of spacecraft trajectories for all events included in our database for MSH crossings between 2017 and 2021 are illustrated in Figure 6. In Figure 6a we show that the C4 crossings of the magnetosheath are equally distributed between the flanks; the M4 crossings are mostly located in the dawn flank. Figures 6b and 6c show that most of the M4 events are located northward of the ecliptic plane ($Z > 0$).

To better understand the distributions in Fig. 6, we also inspected the full spacecraft orbits in 2017-2021 (not shown here). Overall, we determined that Cluster orbits intersecting the magnetosheath have a minimum in Y GSE in June, while the correspond-

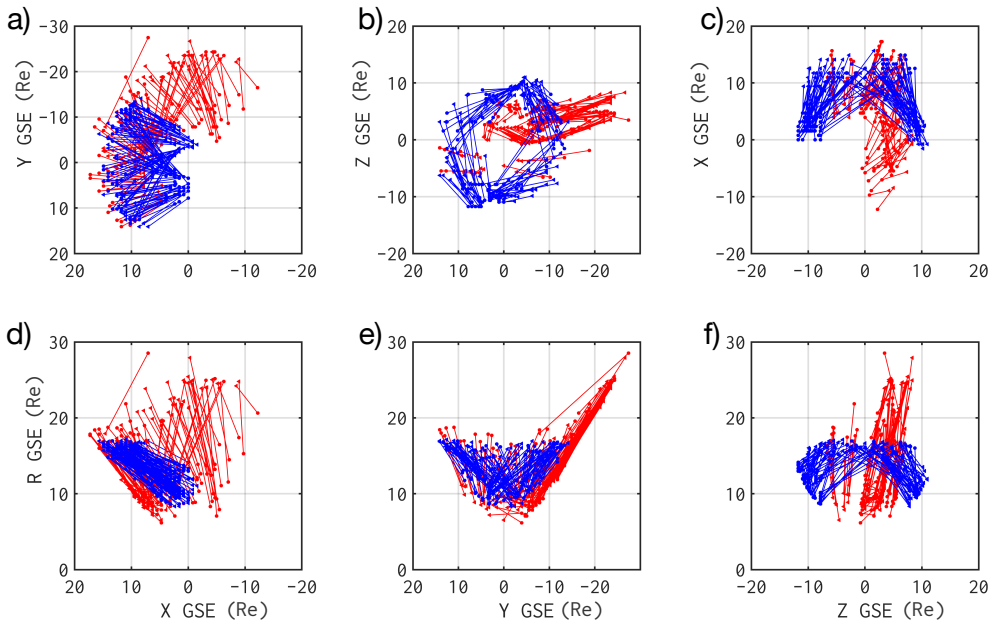

Figure 6. An illustration of M4 and C4 trajectories for all 117 events included in the database. As in previous figures, the M4 spacecraft is depicted in red and C4 is in blue. Only two points are shown per trajectory, the entry and the exit point for the MSH traversal.

ing minimum for MMS is observed for May. More specifically, for Cluster, the minimum values of the Y coordinate reach 0 RE at the beginning of March, and the distribution is skewed towards positive values in Jan-Feb, and towards negative values in March-April; this means that equal intervals of positive and negative Y values are observed. For MMS, we determined that the Y coordinate is skewed towards positive values only in January, and towards negative values for the rest of the interval. This means that MMS spacecraft spend a much larger amount of time at negative Y values, compared to Cluster.

We also calculated the total distance between C4 and M4 spacecraft for all 117 events included in our database (not illustrated). The distance was calculated at a time stamp corresponding to the middle of each interval of simultaneous MSH observations. We found that the distance between C4 and M4 ranges from 1.48 RE (for event 202104ev03) to 27.83 RE (for event 202001ev04). The distribution of inter-spacecraft distances is Gaussian, with an average distance equal to 13.53 RE and a median value equal to 13.42 RE. We also determined that a number of 21 events (18%) are conjunctions (with separation distance less than 8 RE) and a number of 24 events (21%) are oppositions (with distance larger than 18 RE).

4.2 An Overview of Bow Shock Orientation Estimated for Magnetosheath Crossings Included in the Cluster-MMS Database

A sensible exercise that is noteworthy, consists in an analysis of the bow shock geometries estimated through the two methods mentioned above, the MVAB and the geometrical approach, respectively. A direct comparison between the results provided by the two methods is not very relevant as MVAB results in a quasi-instantaneous estimation of the bow shock geometry at the traversal time while the geometrical model-based method gives an estimation of the geometry for the entire time interval, allowing for a

448 characterization of the bow shock geometry for longer periods of time. Nevertheless, some
449 statistics of this analysis are interesting to point out. In Table 2 we show the distribu-
450 tion of bow shock orientations for the entire collection of 117 events included in the database.
451 We define three classes of results obtained with the MVAB approach: (1) quasi-parallel
452 ($Q_{\parallel}$), (2) quasi-perpendicular ($Q_{\perp}$) and (3) "Missing". The two classes $Q_{\parallel}$ and $Q_{\perp}$ are
453 estimated using the average values of the instantaneous θ_{Bn} values calculated with MVAB
454 over an interval of one hour centered on each bow shock crossing. The events labeled as
455 "Missing", are those for which no clear bow shock crossing could be determined by vi-
456 sual inspection of in-situ magnetic field observations.

457 In February-March 2017, the MMS spacecraft underwent an apogee-raising cam-
458 paign. The spacecraft apogee was increased from 12 to 25 Earth radii. We identified 41
459 events in 2017, and for most of them, the spacecraft did not cross the bow shock into
460 the solar wind, but instead remained in the magnetosheath at apogee. This is the rea-
461 son why 17 events are classified as "missing". In total, the MVAB analysis of C4 data
462 identifies 76 events in class $Q_{\perp}$, 41 events in class $Q_{\parallel}$. On the other hand the MVAB anal-
463 ysis of MMS 4 data finds 62 events in class $Q_{\perp}$ and 38 events in class $Q_{\parallel}$. Note that $\sim$
464 65% of the C4 crossing of the MSH in our database are classified as $Q_{\perp}$ by MVAB, and
465 only $\sim 35\%$ are $Q_{\parallel}$.

466 A similar exercise was performed on the results provided by the second approach,
467 based on geometrical arguments and models of the bow shock. The criterion used to de-
468 fine the $Q_{\parallel}$ and $Q_{\perp}$ classes was relaxed to 50%, meaning that if θ_{Bn} takes values between
469 45° and 135° for at least 50% of the MSH crossing, the interval is classified as $Q_{\perp}$. The
470 crossing is considered quasi-parallel if for more than 50% of the time interval θ_{Bn} is out-
471 side those limits. If there is no dominant geometry during the analyzed interval, the event
472 is classified as "mixed". With this approach we find that 72 MSH crossings by C4 fall
473 into the $Q_{\perp}$ class; for 31 crossings we find a quasi-parallel geometry. The same analy-
474 sis applied on M4 data shows that 56 crossings pertain to the $Q_{\perp}$ class while 50 cross-
475 ings pertain to the quasi-parallel case. Note also that $\sim$ 62% of C4 crossing are clas-
476 sified as $Q_{\perp}$ by the model, and only $\sim 26\%$ are classified as $Q_{\parallel}$.

477 A rather unexpected observation is that the $Q_{\perp}$ geometry seems to be more often
478 observed, with a good agreement between the two methods. It is beyond the scope of
479 this paper to investigate the sources of the imbalance, yet we are aware of several pos-
480 sible causes. A mostly radial IMF could have an effect on our determinations consider-
481 ing that a large number of events are recorded in the flanks, relatively far from the bow
482 shock nose, configurations that favor a $Q_{\perp}$ geometry when the IMF is radial (see, e.g.,

Table 2. Number of events distributed according to bow shock orientation. In addition to $Q_{\parallel}$ and $Q_{\perp}$, column "MVAB-missing" includes events for which no clear bow shock crossing could be determined. Column "Model-mixed" includes events for which there is no dominant geometry. C4 is in blue, and MMS4 is in red (see text for details).

Year	MVAB			Model		
	$Q_{\perp}$	$Q_{\parallel}$	Missing	$Q_{\perp}$	$Q_{\parallel}$	Mixed
2017	28/17	13/7	0 /17	27/19	10/16	4 /6
2018	15/14	9 /10	0 /0	18/13	3 /9	3 /2
2019	9 /8	9 /10	0 /0	7 /6	8 /11	3 /1
2020	10/12	5 /3	0 /0	7 /7	6 /7	2 /1
2021	14/11	5 /8	0 /0	13/4	11/7	2 /1
Total	76/62	41/38	0 /17	72/56	31/50	14/11

Fig. 1 in Vuorinen et al., 2019). The relative imbalance between $Q_\perp$ and $Q_\parallel$ geometry can also be related to spacecraft orbits. Liebert et al. (2018) performed a statistical survey of bow shock observations from Cluster, and found a similar imbalance, with the majority of their events being $Q_\perp$; they argued that their event selection procedure caused this imbalance. This should not be the case for our collection, since we selected entire magnetosheath intervals, and not just individual bow shock or magnetopause crossings. Nevertheless, the selection criteria used to build the database of simultaneous Cluster-MMS measurements might, itself, introduce a systematic error. As described in Section 3.1 and shown in Figure 3, an important number of MSH crossings by C4 and M4 lack a common time interval and therefore are discarded from our database, which can have an impact on the statistics of various geometries.

Also, in general, a $Q_\perp$ bow shock is easily identifiable as opposed to $Q_\parallel$ geometry, where it is rather hard to determine the exact location of the bow shock. This fact has direct effects on the MVAB analysis: by translating the analysis window only by minutes, a different result could be obtained. In such cases, maybe a geometrical estimation of the geometry is more suited. However, the model-based method has its own limitations. In the approach we adopted here, the bow shock curve and the normal position are fixed for the entire MSH crossing. For longer crossings, of several hours, these parameters might also vary, especially in the case of MMS, where the Y coordinate changes significantly. One way to diminish such effects would be to recompute the normal to the bow shock at different positions of the spacecraft during its excursion through the MSH.

Another interesting point shown in Table 2 is that around $\sim 10\%$ of events are classified by the model-based method as mixed, for both MMS and Cluster. When the threshold on the amount of time for θ_{Bn} to take values within the pre-defined interval is increased from 50% to 85% the number of mixed events increases to more than 50%.

5 Summary and Conclusions

We report the results of a study which searched for joint observations of the magnetosheath by Cluster and MMS; the study led to building a catalogue of simultaneous MSH crossings identified between 2017 and 2021. We focused on the C4 and M4 probes, but the small inter-spacecraft separations within each quartet allows for a relatively quick expansion to other Cluster-MMS pairs.

Magnetosheath intervals were identified using visual inspection of data summary plots provided by the respective missions. The identification procedure was based mainly on the inspection of ion energy spectra and magnetic field observations, which show clearly identifiable changes when a spacecraft crosses from one plasma region to another. Orbit summary plots were also inspected, in order to confirm the dayside location of each spacecraft. As an example, we describe in detail one case of simultaneous crossings of the MSH by Cluster 4 and MMS 4 spacecraft. All available data summary plots available from Cluster and MMS in January-April for each year between 2017 and 2021 were inspected, and a number of 117 simultaneous joined magnetosheath crossing events were identified. We determined that 30% of events are conjunctions in the dawn flank, 10% are conjunction at dusk, 20 events are oppositions, and about 40 events include crossings from one flank to the other.

For all events included in our catalogue we estimate the bow shock geometry using two complementary methods: a) minimum variance analysis of the magnetic field, and b) geometrical considerations with respect to a model bow shock (Farris et al., 1991). We compared the results obtained with the two methods and find that in about 75% of the cases both methods estimate the same bow shock geometry. The MVAB analysis of C4 data identifies 76 quasi-perpendicular MSH crossings; 41 events satisfy the condition for a quasi-parallel geometry. For the M4 data, the MVAB analysis finds 62 $Q_\perp$ cross-

533 ings and 38 $Q_{\parallel}$ ones. On the other hand, the geometrical approach applied on Cluster
534 data suggests that 72 MSH crossings correspond to a $Q_{\perp}$ geometry while 31 crossings
535 satisfy the conditions for $Q_{\parallel}$ geometry. The same analysis applied on MMS 4 data shows
536 that 56 crossings pertain to the $Q_{\perp}$ class while 50 crossings pertain to the $Q_{\parallel}$ one.

537 Our catalogue provides a database of time intervals when Cluster and MMS are
538 simultaneously probing in-situ the Earth's magnetosheath. The catalogue is designed to
539 facilitate two main types of investigations: a) studies of processes/events using Cluster-
540 MMS conjunctions, i.e., when the two constellations are in the same magnetospheric flank,
541 and b) studies of dawn-dusk asymmetries, using the simultaneous opposition of the two
542 constellations with respect to the Sun-Earth line. This paper, as well as the detailed anal-
543 yses included in the database, also includes an analysis of spacecraft trajectories dur-
544 ing each event. The data and analysis results included in the catalogue can further help
545 future studies devoted, for instance, to search for magnetosheath jets.

546 The catalogue and all associated figures and tables are uploaded to an independent
547 online data repository (Munteanu & Teodorescu, 2024), and can be freely downloaded
548 and used by any interested researcher.

549 Open Research Section

550 The main objective of this work was the creation of a catalogue of simultaneous
551 Cluster-MMS magnetosheath crossings in 2017-2021. The catalogue comprises 117 events,
552 and is available for download through our project TWISTER (http://www.spacescience
553 .ro/projects/twister), and from Zenodo: https://doi.org/10.5281/zenodo.10782134.
554 This study used Cluster quicklook images from http://www.cluster.rl.ac.uk/csdsweb
555 -cgi/csdsweb_pick, and spin resolution data from the fluxgate magnetometer onboard
556 Cluster 4 from https://cdaweb.gsfc.nasa.gov/cgi-bin/eval2.cgi?dataset=C4_CP
557 _FGM_SPIN&index=sp_phys. MMS quicklook images are available from https://lasp.colorado
558 .edu/mms/sdc/public/plots/#/quicklook, and the MMS "Historical Orbit Plots" can
559 be found at https://lasp.colorado.edu/mms/sdc/public/plots/#/historical-orbit.
560 We also used survey data from the Fluxgate Magnetometer onboard MMS 4 from https://
561 cdaweb.gsfc.nasa.gov/cgi-bin/eval2.cgi?dataset=MMS4_FGM_SRVY_L2&index=sp
562 _phys. Earth's bow shock orientation was estimated using models parameterized with
563 high resolution OMNI data, available from https://cdaweb.gsfc.nasa.gov/cgi-bin/
564 eval2.cgi?dataset=OMNI_HRO2_1MIN&index=sp_phys.

565 Acknowledgments

566 This work was supported by the Romanian Ministry of Research, Innovation and Dig-
567 italization through UEFISCDI Project TWISTER (Contract no. PN-III-P1-1.1-TE-2021-
568 0102), by the Romanian National Core Program LAPLAS VII (Contract no. 30N/2023),
569 and by the European Space Agency PRODEX Project MISSION (No. PEA4000134960).
570 M.E. acknowledges support from the Belgian Solar Terrestrial Center of Excellence (STCE)
571 and from the Belgian Research Action through Interdisciplinary Networks (BRAIN-BE)
572 2.0 (Grant No. B2/223/P1/PLATINUM) funded by the Belgian Office for Research (BEL-
573 SPO).

574 References

575 Alexandrova, O., Carbone, V., Veltri, P., & Sorriso-Valvo, L. (2008). Small-Scale
576 Energy Cascade of the Solar Wind Turbulence. *The Astrophysical Journal*,
577 *674*(2), 1153. doi: https://dx.doi.org/10.1086/524056
578 Balogh, A., Carr, C. M., Acuña, M. H., Dunlop, M. W., Beek, T. J., Brown, P.,
579 ... Schwingenschuh, K. (2001). The Cluster Magnetic Field Investigation:
580 overview of in-flight performance and initial results. *Annales Geophysicae*, *19*,

1207-1217. doi: 10.5194/angeo-19-1207-2001

Balogh, A., & Lucek, A. (2021). [Dataset] Cluster-Tango Spin Resolution Fluxgate Magnetometer (FGM) Data. *NASA*. Retrieved from `hpde.io/ESA/NumericalData/Cluster-Tango/FGM/SpinResolution/PT4S`

Breuillard, H., Matteini, L., Argall, M. R., Sahraoui, F., Andriopoulou, M., Contel, O. L., ... Cohen, I. J. (2018). New Insights into the Nature of Turbulence in the Earth's Magnetosheath Using Magnetospheric MultiScale Mission Data. *The Astrophysical Journal*, *859*(2), 127. doi: https://doi.org/10.3847/1538-4357/aabae8

Burch, J. L., Moore, T. E., Torbert, R. B., & Giles, B. L. (2016). Magnetospheric Multiscale overview and science objectives. *Space Science Reviews*, *199*, 5–21. doi: https://doi.org/10.1007/s11214-015-0164-9

Czaykowska, A., Bauer, T. M., Treumann, R. A., & Baumjohann, W. (2001). Magnetic field fluctuations across the Earth's bow shock. *Annales Geophysicae*, *19*, 275-287. doi: https://doi.org/10.5194/angeo-19-275-2001

Dimmock, A. P., & Nykyri, K. (2013). The statistical mapping of magnetosheath plasma properties based on themis measurements in the magnetosheath interplanetary medium reference frame. *Journal of Geophysical Research: Space Physics*, *118*(8), 4963-4976. doi: https://doi.org/10.1002/jgra.50465

Dimmock, A. P., Pulkkinen, T. I., Osmane, A., & Nykyri, K. (2016). The dawn-dusk asymmetry of ion density in the dayside magnetosheath and its annual variability measured by THEMIS. *Annales Geophysicae*, *34*, 511-528. doi: https://doi.org/10.5194/angeo-34-511-2016

Dumitru, D., & Munteanu, C. (2023). Classifying interplanetary discontinuities using supervised machine learning. *Earth and Space Science*, *10*(7), e2023EA002960. doi: https://doi.org/10.1029/2023EA002960

Dwivedi, N. K., Kumar, S., Kovacs, P., Yordanova, E., Echim, M., Sharma, R. P., ... Sasunov, Y. (2019). Implication of kinetic Alfvn waves to magnetic field turbulence spectra: Earth's magnetosheath. *Astrophys Space Sci*, *364*(101). doi: https://doi.org/10.1007/s10509-019-3592-2

Echim, M., Chang, T., Kovacs, P., Wawrzaszek, A., Yordanova, E., Narita, Y., ... Consolini, G. (2021). Turbulence and Complexity of Magnetospheric Plasmas. In *Magnetospheres in the solar system* (p. 67-91). American Geophysical Union (AGU). doi: https://doi.org/10.1002/9781119815624.ch5

Echim, M., Munteanu, C., Voitcu, G., & Teodorescu, E. (2024). Magnetopause properties at the dusk magnetospheric flank from global magnetohydrodynamic simulations, the kinetic Vlasov equilibrium, and in situ observations – Potential implications for SMILE. *Earth Planet. Phys.*, *8*(1), 1-12. doi: https://doi.org/10.26464/epp2023066

Echim, M., Voiculescu, M., Munteanu, C., Teodorescu, E., Voitcu, G., Negrea, C., ... Danila, E. (2023). On the phenomenology of magnetosheath jets with insight from theory, modelling, numerical simulations and observations by Cluster spacecraft. *Front. Astron. Space Sci.*, *10*. doi: https://doi.org/10.3389/fspas.2023.1094282

Escoubet, C. P., Fehringer, M., & Goldstein, M. (2001). Introduction: The Cluster mission. *Annales Geophysicae*, *19*(10/12), 1197–1200. doi: https://doi.org/10.5194/angeo-19-1197-2001

Escoubet, C. P., Hwang, K.-J., Toledo-Redondo, S., Turc, L., Haaland, S. E., Aunai, N., ... Torbert, R. B. (2020). Cluster and MMS Simultaneous Observations of Magnetosheath High Speed Jets and Their Impact on the Magnetopause. *Frontiers in Astronomy and Space Sciences*, *6*. doi: https://doi.org/10.3389/fspas.2019.00078

Farris, M. H., Petrinec, S. M., & Russell, C. T. (1991). The thickness of the magnetosheath: Constraints on the polytropic index. *Geophysical Research Letters*, *18*(10), 1821-1824. doi: https://doi.org/10.1029/91GL02090

Farris, M. H., & Russell, C. T. (1994). Determining the standoff distance of the bow shock: Mach number dependence and use of models. *Journal of Geophysical Research: Space Physics*, *99*(A9), 17681-17689. doi: https://doi.org/10.1029/94JA01020

Fuselier, S. A., Lewis, W. S., Schiff, C., Ergun, R., Burch, J. L., Petrinec, S. M., & Trattner, K. J. (2016). Magnetospheric Multiscale Science Mission Profile and Operations. *Space Science Reviews*, *199*, 77-103. doi: https://doi.org/10.1007/s11214-014-0087-x

Haaland, S., Hasegawa, H., Paschmann, G., Sonnerup, B., & Dunlop, M. (2021). 20 Years of Cluster Observations: The Magnetopause. *Journal of Geophysical Research: Space Physics*, *126*(8), e2021JA029362. doi: https://doi.org/10.1029/2021JA029362

Haaland, S., Paschmann, G., ieroset, M., Phan, T., Hasegawa, H., Fuselier, S. A., ... Burch, J. (2020). Characteristics of the Flank Magnetopause: MMS Results. *Journal of Geophysical Research: Space Physics*, *125*(3), e2019JA027623. doi: https://doi.org/10.1029/2019JA027623

Haaland, S., Reistad, J., Tenfjord, P., Gjerloev, J., Maes, L., DeKeyser, J., ... Dorville, N. (2014). Characteristics of the flank magnetopause: Cluster observations. *Journal of Geophysical Research: Space Physics*, *119*(11), 9019-9037. doi: https://doi.org/10.1002/2014JA020539

Haaland, S., Runov, A., Artemyev, A., & Angelopoulos, V. (2019). Characteristics of the Flank Magnetopause: THEMIS Observations. *Journal of Geophysical Research: Space Physics*, *124*(5), 3421-3435. doi: https://doi.org/10.1029/2019JA026459

Huang, S. Y., Hadid, L. Z., Sahraoui, F., Yuan, Z. G., & Deng, X. H. (2017). On the Existence of the Kolmogorov Inertial Range in the Terrestrial Magnetosheath Turbulence. *The Astrophysical Journal Letters*, *836*(1). doi: https://doi.org/10.3847/2041-8213/836/1/L10

Karlsson, T., Raptis, S., Trollvik, H., & Nilsson, H. (2021). Classifying the magnetosheath behind the quasi-parallel and quasi-perpendicular bow shock by local measurements. *Journal of Geophysical Research: Space Physics*, *110*(A02104). doi: https://doi.org/10.1029/2021JA029269

King, J. H., & Papitashvili, N. E. (2005). Solar wind spatial scales in and comparisons of hourly Wind and ACE plasma and magnetic field data. *Journal of Geophysical Research*, *110*(A02104). doi: https://doi.org/10.1029/2004JA010649

Kolmogorov, A. N. (1941). The local structure turbulence in incompressible viscous fluids for very large Reynolds numbers. *Doklady Akademii Nauk SSSR*, *30*, 301-305.

Krasnoselskikh, V., Balikhin, M., Walker, S., Schwartz, S., Sundkvist, D., Lobzin, V., ... Comisel, H. (2013). The Dynamic Quasi-perpendicular Shock: Cluster Discoveries. *Space. Sci. Rev.*, *178*, 535-598. doi: https://doi.org/10.1007/s11214-013-9972-y

Kruparova, O., Krupar, V., Safrankova, J., Nemecek, Z., Maksimovic, M., Santolik, O., ... Merka, J. (2019). Statistical Survey of the Terrestrial Bow Shock Observed by the Cluster Spacecraft. *Journal of Geophysical Research: Space Physics*, *124*(3), 1539-1547. doi: https://doi.org/10.1029/2018JA026272

Leroy, M. M., Winske, D., Goodrich, C. C., Wu, C. S., & Papadopoulos, K. (1982). The structure of perpendicular bow shocks. *Journal of Geophysical Research: Space Physics*, *87*(A7), 5081-5094. doi: https://doi.org/10.1029/JA087iA07p05081

Li, H., Jiang, W., Wang, C., Verscharen, D., Zeng, C., Russell, C. T., ... Burch, J. L. (2020). Evolution of the Earth's magnetosheath turbulence: a statistical study based on MMS observations. *The Astrophysical Journal Letters*, *898*(2), L43. doi: https://doi.org/10.3847/2041-8213/aba531

Liebert, E., Nabert, C., & Glassmeier, K.-H. (2018). Statistical survey of dayside magnetospheric current flow using Cluster observations: bow shock. *Annales Geophysicae*, *36*(4), 1073-1080. doi: https://doi.org/10.5194/angeo-36-1073-2018

Mailyan, B., Munteanu, C., & Haaland, S. (2008). What is the best method to calculate the solar wind propagation delay? *Annales Geophysicae*, *26*, 2383-2394. doi: https://doi.org/10.5194/angeo-26-2383-2008

Munteanu, C., Haaland, S., Mailyan, B., Echim, M., & Mursula, K. (2013). Propagation delay of solar wind discontinuities: Comparing different methods and evaluating the effect of wavelet denoising. *Journal of Geophysical Research: Space Physics*, *118*(7), 3985–3994. doi: https://doi.org/10.1002/jgra.50429

Munteanu, C., & Teodorescu, E. (2024). [Dataset] A catalogue of simultaneous Cluster-MMS crossings through the Earth's magnetosheath region in January-April, 2017-2021. *Zenodo*. doi: https://doi.org/10.5281/zenodo.10782134

Narita, Y., Plaschke, F., & Vörös, Z. (2021). The Magnetosheath. In *Magnetospheres in the solar system* (chap. 9). American Geophysical Union (AGU). doi: https://doi.org/10.1002/9781119815624.ch9

Papitashvili, N. E., & King, J. H. (2020). [Dataset] OMNI, Combined Solar Wind Plasma Moments and Interplanetary Magnetic Field (IMF) Time-Shifted to the Nose of the Earth's Bow Shock, plus Geomagnetic Indices, 1 min Data. *NASA Space Physics Data Facility*. doi: https://doi.org/10.48322/mj0k-fq60

Paschmann, G., Haaland, S. E., Phan, T. D., Sonnerup, B. U. ., Burch, J. L., Torbert, R. B., ... Fuselier, S. A. (2018). Large-Scale Survey of the Structure of the Dayside Magnetopause by MMS. *Journal of Geophysical Research: Space Physics*, *123*(3), 2018-2033. doi: https://doi.org/10.1002/2017JA025121

Plank, J., & Gingell, I. L. (2023). Intermittency at Earth's bow shock: Measures of turbulence in quasi-parallel and quasi-perpendicular shocks. *Physics of Plasmas*, *30*(082906). doi: https://doi.org/10.1063/5.0160439

Rakhmanova, L., Riazantseva, M., & Zastenker, G. (2021). Plasma and Magnetic Field Turbulence in the Earth's Magnetosheath at Ion Scales. *Frontiers in Astronomy and Space Sciences*, *7*. doi: https://doi.org/10.3389/fspas.2020.616635

Rème, H., Aoustin, C., Bosqued, J. M., Dandouras, I., Lavraud, B., Sauvaud, J. A., ... Sonnerup, B. (2001). First multispacecraft ion measurements in and near the Earth's magnetosphere with the identical Cluster ion spectrometry (CIS) experiment. *Annales Geophysicae*, *19*, 1303-1354. doi: 10.5194/angeo-19-1303-2001

Russell, C., Anderson, B., Baumjohann, W., Bromund, K., Dearborn, D., Fischer, D., & Richter, I. (2016). The Magnetospheric Multiscale Magnetometers. *Space Science Reviews*, *199*, 189-256. doi: https://doi.org/10.1007/s11214-014-0057-3

Russell, C., Magnes, W., Wei, H., Bromund, K., Plaschke, F., Fischer, D., ... Burch, J. (2022). [Dataset] MMS 4 Flux Gate Magnetometer (FGM) DC Magnetic Field, Level 2 (L2), Survey Mode, 8 or 16 Samples/s, v4/5 Data. *NASA Space Physics Data Facility*. doi: https://doi.org/10.48322/50p5-d131

Sahraoui, F., Belmont, G., Rezeau, L., Cornilleau-Wehrlin, N., Pinçon, J. L., & Balogh, A. (2006). Anisotropic Turbulent Spectra in the Terrestrial Magnetosheath as Seen by the Cluster Spacecraft. *Phys. Rev. Lett.*, *96*, 075002. doi: https://link.aps.org/doi/10.1103/PhysRevLett.96.075002

Schwartz, S. J., & Burgess, D. (1991). Quasi-parallel shocks: A patchwork of three-dimensional structures. *Geophysical Research Letters*, *18*(3), 373-376. doi: https://doi.org/10.1029/91GL00138

Shen, C., Dunlop, M., Li, X., Liu, Z. X., Balogh, A., Zhang, T. L., ... Chen, Z. Q. (2007). New approach for determining the normal of the bow shock based on Cluster four-point magnetic field measurements. *Journal of Geophysical Re-*

search: Space Physics, *112*(A3). doi: https://doi.org/10.1029/2006JA011699

Shevyrev, N., Zastenker, G., Eiges, P., & Richardson, J. (2006). Low frequency waves observed by Interball-1 in foreshock and magnetosheath. *Advances in Space Research*, *37*(8), 1516-1521. doi: https://doi.org/10.1016/j.asr.2005.07.072

Smith, C. W., Hamilton, K., Vasquez, B. J., & Leamon, R. J. (2006). Dependence of the Dissipation Range Spectrum of Interplanetary Magnetic Fluctuations on the Rate of Energy Cascade. *The Astrophysical Journal*, *645*(1), L85. doi: https://dx.doi.org/10.1086/506151

Song, P., & Russell, C. (1997). What do we really know about the magnetosheath? *Advances in Space Research*, *20*(4), 747-765. doi: https://doi.org/10.1016/S0273-1177(97)00466-3

Sonnerup, B. U. Ö., & Scheible, M. (1998). Minimum and Maximum Variance Analysis. *Analysis Methods for Multi-Spacecraft Data, G. Paschmann, P.W. Daly (Eds.), ISSI Scientific Reports Series, ESA/ISSI*, *1*, 185-220.

Tátrallyay, M., Erdös, G., Németh, Z., Verigin, M. I., & Vennerstrom, S. (2012). Multispacecraft observations of the terrestrial bow shock and magnetopause during extreme solar wind disturbances. *Annales Geophysicae*, *30*(12), 1675-1692. doi: https://doi.org/10.5194/angeo-30-1675-2012

Teodorescu, E., & Echim, M. M. (2020). Open-Source Software Analysis Tool to Investigate Space Plasma Turbulence and Nonlinear DYNamics (ODYN). *Earth and Space Science*. doi: https://doi.org/10.1029/2019EA001004

Teodorescu, E., Echim, M. M., & Voitcu, G. (2021). A Perspective on the Scaling of Magnetosheath Turbulence and Effects of Bow Shock Properties. *The Astrophysical Journal*, *910*(1). doi: https://doi.org/10.3847/1538-4357/abe12d

Vuorinen, L., Hietala, H., & Plaschke, F. (2019). Jets in the magnetosheath: IMF control of where they occur. *Annales Geophysicae*, *37*(4), 689-697. doi: https://doi.org/10.5194/angeo-37-689-2019

Walsh, B. M., Sibeck, D. G., Wang, Y., & Fairfield, D. H. (2012). Dawn-dusk asymmetries in the Earth's magnetosheath. *Journal of Geophysical Research*, *117*(A12211). doi: https://doi.org/10.1029/2012JA018240

Walters, G. K. (1964). Effect of Oblique Interplanetary Magnetic Field on Shape and Behavior of the Magnetosphere. *Journal of Geophysical Research*, *69*(9), 1769-1783. doi: https://doi.org/10.1029/JZ069i009p01769